Room-temperature operation of a radiofrequency diamond magnetometer near the shot-noise limit

Chang S. Shin,[1,2] Claudia E. Avalos,[1,2] Mark C. Butler,[1,2,a)] David R. Trease,[1,2,b)] Scott J. Seltzer,[1,2] J. Peter Mustonen,[1,2,c)] Daniel J. Kennedy,[1,2] Victor M. Acosta,[4,d)] Dmitry Budker,[3,4] Alexander Pines,[1,2] and Vikram S. Bajaj[1,2,e)]

[1]*Materials Sciences Division, Lawrence Berkeley National Laboratory, Berkeley, California 94720, USA*
[2]*Department of Chemistry and California Institute for Quantitative Biosciences, University of California, Berkeley, California 94720, USA*
[3]*Nuclear Science Division, Lawrence Berkeley National Laboratory, Berkeley, California 94720, USA*
[4]*Department of Physics, University of California, Berkeley, California 94720, USA*

(Received 17 October 2012; accepted 31 October 2012; published online 28 December 2012)

We operate a nitrogen-vacancy (NV^-) diamond magnetometer at ambient temperatures and study the dependence of its bandwidth on experimental parameters including optical and microwave excitation powers. A model based on the Bloch equations is used to analyze the NV center's response time, τ, during continuous optical and microwave irradiation, and τ^{-1} is shown to be a weighted average of T_1^{-1} and T_2^{-1}, where T_1 and T_2 are the longitudinal and transverse relaxation times of the electron spin during optical irradiation. We measured a maximum detection bandwidth of ~1.6 MHz with optical excitation intensity of ~2.3 MW/cm^2, limited by the available optical power. The sensitivity of the NV ensemble for continuous-wave magnetometry in the presence of photon shot noise is analyzed. Two detection schemes are compared, one involving modulation of the fluorescence by an oscillating magnetic field while the microwave frequency is held constant, and the other involving double modulation of the fluorescence when the microwave frequency is modulated during the detection. For the first of these methods, we measure a sensitivity of 4.6 ± 0.3 nT/$\sqrt{\text{Hz}}$, unprecedented in a detector with this active volume of ~10 μm^3 and close to the photon-shot-noise limit of our experiment. The measured bandwidth and sensitivity of our device should allow detection of micro-scale NMR signals with microfluidic devices. © *2012 American Institute of Physics*. [http://dx.doi.org/10.1063/1.4771924]

I. INTRODUCTION

The negatively charged nitrogen vacancy center (NV^-), a substitutional point defect in diamond (later denoted as NV throughout the paper), exhibits favorable optical and magnetic properties that have recently been exploited in several applications. For example, their brightness, optical stability, and biological inertness make NV defect-harboring nanodiamonds ideal probes in bioimaging[1] and fluorescence resonance energy transfer[2] experiments. More importantly, the NV defect forms a magneto-optical system whose spin state can be initialized and read out optically. Because the NV spin-coherence lifetimes can be as long as milliseconds in an isotopically pure diamond lattice,[3] the system is an ideal platform for experimental quantum information science. Among such devices are precision magnetometers that have applications as industrial sensors, probes of magnetic materials, and as detectors of magnetic resonance. Practical magnetic-field sensors for electron spin resonance (ESR), nuclear magnetic resonance (NMR), and other similar applications must sensitively detect weak, oscillating magnetic fields whose frequency and bandwidth cannot be arbitrarily controlled. Thus, the transient response of an ensemble of NV centers, characterized by its sensitivity to magnetic fields oscillating over a wide bandwidth, is a critical metric for applications in NMR and magnetic resonance imaging.

Using a single NV center in isotopically pure diamond, a magnetic sensitivity of ~4 nT/$\sqrt{\text{Hz}}$ has recently been reported[3] and an extrapolated (but not measured) sensitivity of ~20 nT/$\sqrt{\text{Hz}}$ using an ensemble of NV centers was also reported,[4] both at ambient temperatures. Infrared-absorption detection, using an NV ensemble, achieved a sensitivity of ~7 nT/$\sqrt{\text{Hz}}$ at 45 K.[5] In that work, a theoretical bandwidth of a few MHz was suggested, but experimental operation was limited to a few hundred Hz. With a single NV center, a detection bandwidth of a several hundred kHz has been reported.[6]

In combination with pulsed decoupling schemes, probes incorporating single NV centers in isotopically pure (i.e., ^{12}C) diamond matrices are ideal for scanning probe magnetometry applications. By contrast, continuous wave NV magnetometry at a larger scale and with an ensemble of NV centers in more readily available diamond matrices (HPHT) is more adapted to industrial applications such as microscale NMR within microfluidic devices. In these applications, the

[a)]Present address: William R. Wiley Environmental Molecular Sciences Laboratory, Pacific Northwest National Laboratory, P.O. Box 999, Richland, Washington 99352, USA.
[b)]Present address: KLA Tencor, Milpitas, California 95035, USA.
[c)]Present address: Alkermes, Inc., 852 Winter Street, Waltham, Massachusetts 02451-1420, USA.
[d)]Present address: Hewlett-Packard Laboratories, Palo Alto, California 94304, USA.
[e)]Author to whom correspondence should be addressed. Electronic mail: vikbajaj@gmail.com.

detector volume is matched to the microfluidic channel; thus, detector sensitivity and bandwidth are much more important variables than spatial resolution.

In general, detector bandwidth is limited by the characteristic time constants of the NV center. We overcome this limit by using optical excitation powers at which the effective T_1 and T_2 of the NV center are shortened by the optical pumping cycle. With an optical excitation intensity of $\sim$2.3 MW/cm^2 (optical excitation intensity refers to the average intensity throughout the paper), limited by the available optical power, we measured bandwidths as large as $\sim$1.6 MHz. With optimized operational parameters, we also measured a sensitivity of $\sim 4.6 \pm 0.3$ nT/$\sqrt{\text{Hz}}$. These measurements used fluorescence detection techniques at room temperature with an active volume of only $\sim$10 μm^3, matched to the size of microfluidic channels and much smaller than is practical with inductive NMR detection techniques. Section II describes the bandwidth and sensitivity measurements, in which we record the fluorescence signal from the NV centers under frequency modulation of the microwave field and/or an oscillating magnetic field. The latter simulates an NMR signal of interest, as shown in Fig. 1. In Sec. III, we study the transient response of an NV center under continuous microwave and optical irradiation, in order to understand the dynamics that limit the bandwidth of the magnetometer. The NV spin system can be modeled as a set of three two-level systems, whose resonant frequencies are separated by $\sim$2.1 MHz due to the hyperfine coupling between the electron spin and the ^{14}N nuclear spin. Since the two-level systems can be considered essentially isolated from each other,[7] Bloch equations are used to model the response of each system individually, with the optically induced spin-relaxation included in the model only through T_1 and T_2, the effective longitudinal and transverse relaxation times under continuous optical excitation, respectively. The Bloch-equation model is used to analyze the NV centers' response time, τ, and τ^{-1} is shown to be a weighted average of T_1^{-1} and T_2^{-1}. The theory is validated by comparison with experiment.

Section IV analyzes the sensitivity limit imposed by photon shot noise of the fluorescence signal from the NV centers. When the microwave field is tuned to a frequency where the slope of the optically detected magnetic-resonance (ODMR) spectrum is maximal, an oscillating magnetic field can be measured by detecting the corresponding oscillations in the fluorescence from the NV-center ensemble, as schematically shown in Fig. 1(b). An alternative measurement method is to modulate the microwave frequency about the center of the ODMR spectrum during the detection of the magnetic field. The oscillations in fluorescence have the functional form $\cos(\omega_m t + \varphi_m)\cos(\omega_c t)$, where ω_c is the frequency of the carrier wave that modulates the microwave frequency, ω_m is the frequency of the oscillating magnetic field, and φ_m depends on the relative phase of the carrier wave and the magnetic field. Demodulation using a lock-in

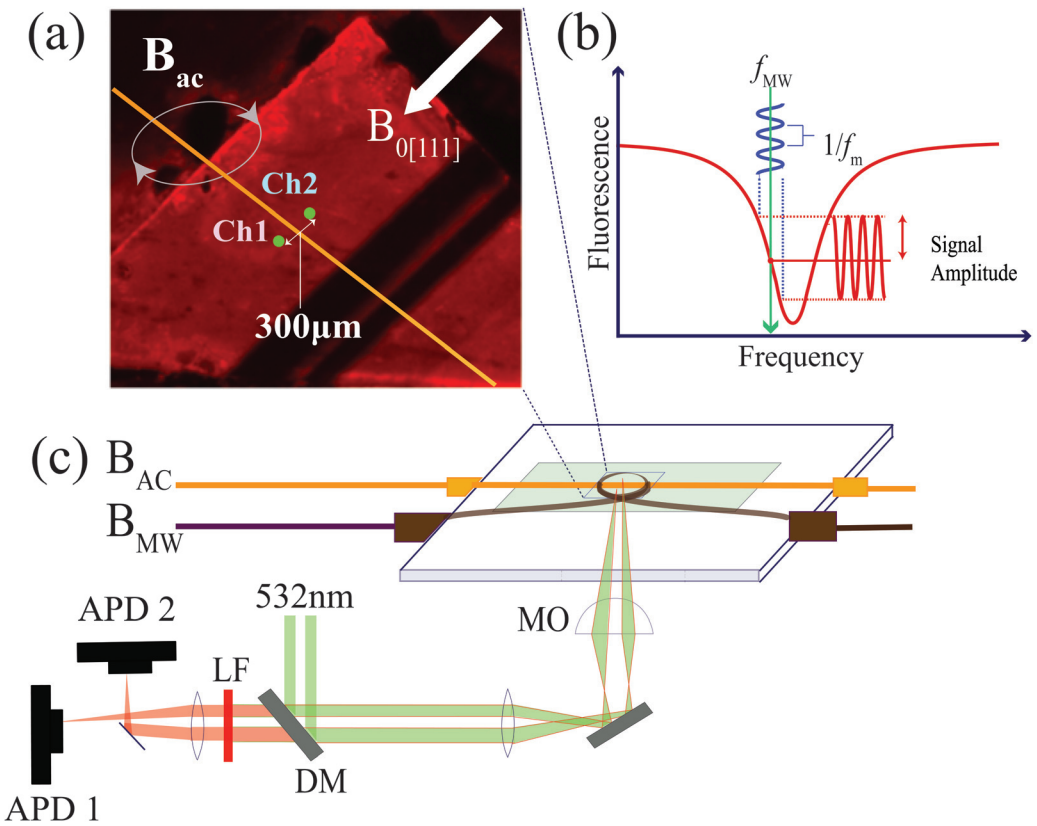

FIG. 1. (a) Fluorescence image of the diamond and a representation of the thin wire (80 μm diameter), which is used to produce small oscillating magnetic fields. A similar wire was used to produce the microwave field. A three-axis set of Helmholtz coils was used to produce B_0, while B_{MW} was generated using a high frequency microwave source. The oscillating field B_{AC} from the 80-μm OD wire was produced using a function generator. (b) Schematic of modulated fluorescence detection technique, where frequency-modulated MW is applied. (c) Schematic of experimental setup. MO refers to the 20X microscope objective with NA of 0.4, and LF and DM are a long-pass filter (cut-off at 650 nm) and a dichroic mirror, respectively, and APD stands for avalanche photodetector. The two excitation spots (shown in the inset) were separated by $\sim$300 μm. The green refers to the 532 nm excitation, red to the fluorescence signal.

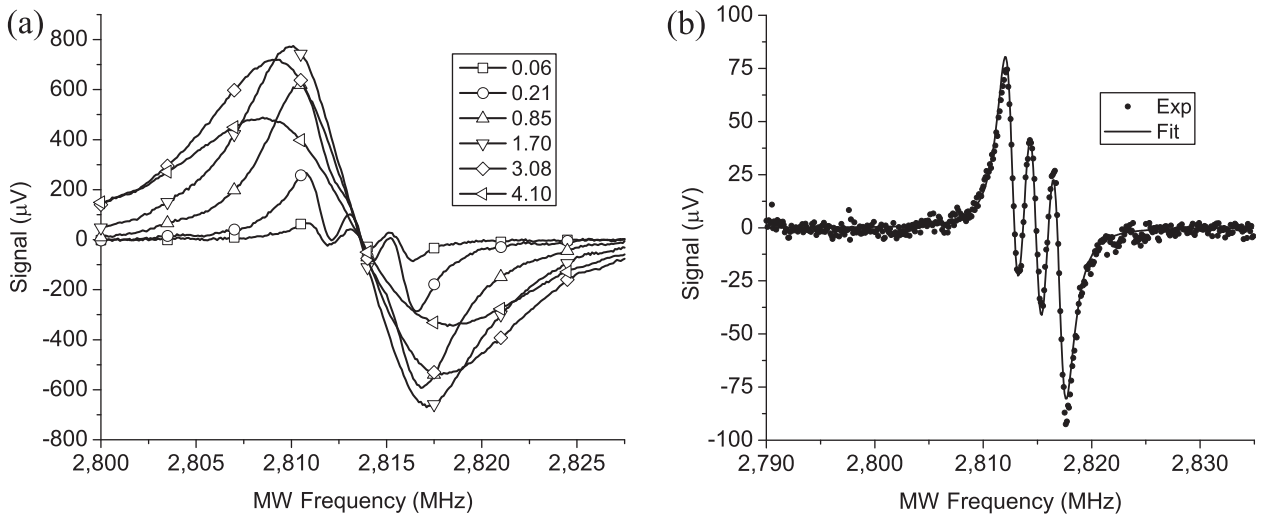

FIG. 2. (a) Derivative spectra at optical excitation intensity of 2.3 MW/cm^2 with various Rabi frequencies ($\omega_1/2\pi$), indicated in MHz in the figure. Center frequency shift due to heating effects was compensated for in the plot. All derivative spectra were measured with a microwave modulation amplitude of 250 kHz at a microwave modulation rate of 25 kHz. (b) A closeup of the curve for Rabi frequency of 0.06 MHz with an additional fit. Black circles indicate the experimental data, and the solid line shows a fit to the derivative of three summed Lorentzian line shape functions. Estimated T_2^* from the ODMR spectrum was 130 ± 5 ns.

amplifier and a spectrum analyzer in sequence yields an estimate of the magnetic field. We will refer to these two measurement techniques as single-modulation and double-modulation methods, respectively, due to the modulation they induce in the fluorescence. Consistent with the analysis, experimental tests show that the single-modulation method is preferred if the effects of low-frequency fluctuations in laser power are eliminated, for example, by the use of a gradiometer configuration. For measurements performed using the single-modulation method, the sensitivity of the diamond magnetometer was near the shot-noise limit.

II. DEVICE OPERATION

The diamond sample in our experiments is S9 (NV concentration of ~2 ppm) described in Ref. 8, and the geometry of our experiment is illustrated in Fig. 1(c). The NV center ground state is a spin triplet (S = 1) with zero field splitting of 2.87 GHz between sublevels $m_s = 0$ and $m_s = \pm 1$. For ODMR experiments, a static magnetic field of ~20 G was applied along the [111] crystal orientation to break the orientational degeneracy of the NV center. The static field also shifts the transition between $m_s = 0$ and $m_s = +1$ out of resonance with the applied microwave field that is matched to the transition between $m_s = 0$ and $m_s = -1$. The experiments generally probed a single manifold of resolved hyperfine lines.[4] Microwaves were applied to the NV spins using a wire loop of inner diameter 1.5 mm, placed close to the diamond surface (described fully in the figure captions). Derivative spectra were obtained by applying a frequency modulated microwave signal at various microwave powers, as shown in Fig. 2(a), and T_2^* was estimated to be 130 ± 5 ns, as seen in Fig. 2(b).

A. Bandwidth measurement

The frequency response of the NV ensemble at a given optical and microwave power was obtained by applying frequency-modulated microwaves at the peak of the derivative spectrum, i.e.,

$$f_{mw}(t) = f_{peak} + \Delta f \cdot \cos(2\pi \cdot f_m \cdot t + \varphi),$$

where f_{mw} is the instantaneous microwave frequency, centered at f_{peak}, and f_m is the modulation rate, which was varied from 1 kHz to 2 MHz with a constant modulation amplitude $\Delta f = 1$ MHz. The modulated signal, normalized to the peak amplitude was plotted as a function of modulation rate, as seen in Figs. 3 and 4.

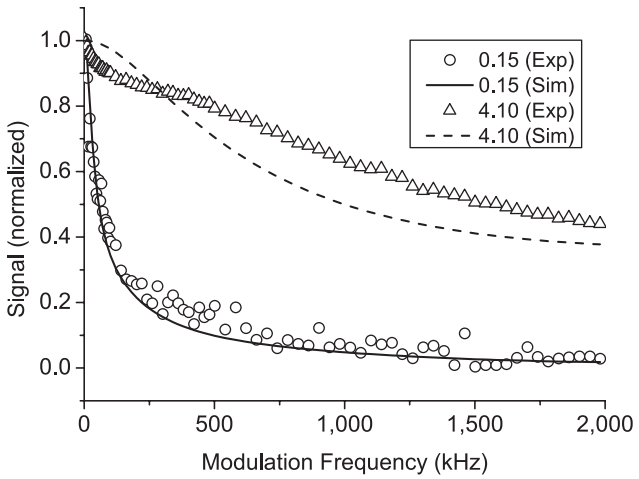

FIG. 3. Comparison of simulation and experiment for a bandwidth measurement at laser intensity of 1.95 MW/cm^2 and microwave field strengths, corresponding to $\omega_1/2\pi = 0.10$ MHz and 4.10 MHz, respectively. For $\omega_1/2\pi = 0.15$ MHz, the central microwave frequency was set to a resolved hyperfine peak at the edge of the derivative spectrum, which offset the microwave frequency by 0.6 MHz from the the nearest resonance of the ODMR spectrum. The magnetometer response at a given rate ω_m was characterized using frequency modulation of the microwave field with amplitude 1.0 MHz and modulation rate ω_m. The experimentally measured time constants used for the two NV-center ensemble simulation, described in Sec. III, were $T_1 = 7.0$ μs and $T_1 = 1.1$ μs (obtained from a biexponential fit to a repolarization curve), and $T_2 = 150$ ns. For $\omega_1/2\pi = 4.10$ MHz, the hyperfine splittings were not resolved, and the offset from resonance was 3.0 MHz. The modulation amplitude used for the measurement, as well as the time constants T_1, T_2 used for the simulation, were the same as for $\omega_1/2\pi = 0.15$ MHz case. (Numbers in the figure correspond to the Rabi frequencies, and Exp and Sim refer to the experimental data and simulation data, respectively.)

In order to qualitatively understand how the dynamics of the ensemble NV centers under continuous optical and microwave excitation depends on experimental parameters, we first measured the T_1 of 462.6 μs and T_2 of 2.0 μs in the absence of optical excitation. Measurements of T_1 and T_2 were repeated under continuous optical excitation at various powers, and the ensemble T_1 and T_2 were found to decrease significantly as optical power increased, due to faster repolarization. For example, at an optical excitation intensity of $\sim$0.3 MW/cm^2, estimated from the measured power before the microscope objective and the diffraction limited spot size, the ensemble T_1 is $\sim$ 11.0 μs and T_2 is $\sim$ 1.0 μs, decreasing to 2.2 μs and 140 ns, respectively, at $\sim$2.0 MW/cm^2. This dramatic change in the measured time constants, T_1 and T_2 suggests that the Gaussian profile of the beam introduces significant spatial inhomogeneity in T_1 and T_2. As the microwave power is increased, we can expect that the full ensemble of NV centers, inhomogeneously illuminated by the laser, will contribute to the dynamics, with each NV center having a different transient response and fluorescence intensity. In order to account for the spatial inhomogeneity of the laser intensity in simulations, we include two sets of T_1 and T_2 values, which is later referred to as the 'two NV center' simulation in Sec. III, to serve as a simple model of multiple classes of NV centers.

In Fig. 5, we illustrate similar experiments repeated at various optical and microwave excitation powers, along with estimated bandwidths, defined as the modulation rate at which the amplitude decreases by 3 dB. At an optical excitation intensity of $\sim$2.3 MW/cm^2, the measured bandwidth increased to $\sim$1.6 MHz as $\omega_1/2\pi$, the Rabi frequency associated with the resonant component of the microwave field, was increased to 4.10 MHz. At a lower optical excitation intensity of 0.02 MW/cm^2, the bandwidth increased only to $\sim$39 kHz when $\omega_1/2\pi$ was increased over the same range.

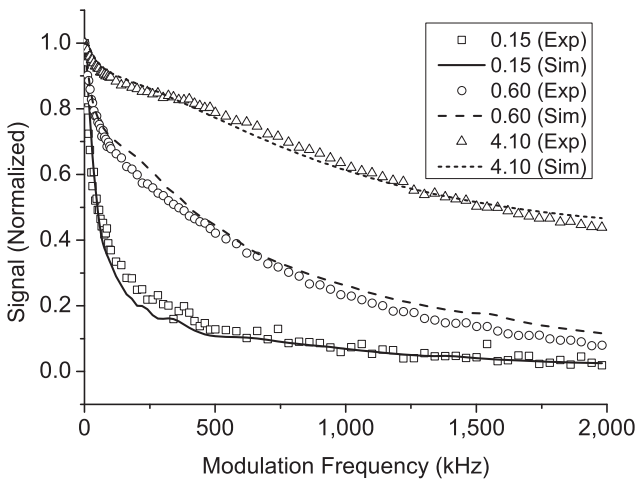

FIG. 4. Representative experimental data together with simulation data at an optical excitation intensity of 1.95 MW/cm^2. Unlike Fig. 3, this simulation with 2 NV-center ensemble, use two sets of T_1 and T_2, i.e., $T_1 = 15$ μs, $T_2 = 1.5$ μs and $T_1 = 0.5$ μs, $T_2 = 0.1$ μs, which are NOT based on the measured values but adjusted to fit the data. (Numbers in the figure correspond to the Rabi frequencies, and Exp and Sim refer to the experimental data and simulation data, respectively.)

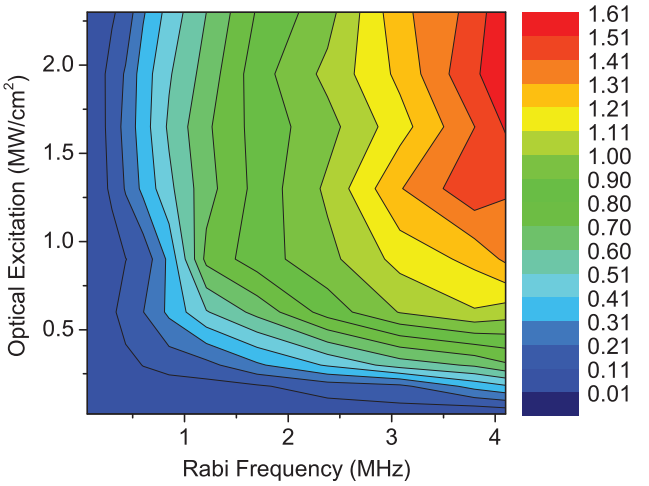

FIG. 5. Experimentally estimated bandwidth in MHz is plotted as a function of the optical excitation intensity and the microwave Rabi frequency. The system shows saturation behavior at $\sim$0.6 MW/cm^2 of optical excitation intensity, for $\omega_1/2\pi > 2.0$ MHz.

B. Sensitivity measurement

In sensitivity measurements using the single-modulation technique, microwave excitation was applied at the frequency where the slope of the ODMR spectrum is maximal, a small magnetic field at 2 kHz was applied to the ensemble of NV centers within the excitation spot, and the modulated fluorescence signal was integrated for 1 sec using a spectrum analyzer (Stanford Research 770) with a uniform window function. In the gradiometer configuration, two 532 nm beams were used to excite NV centers in two distinct spots, separated by $\sim$ 300 μm in the diamond sample. In principle, the gradiometer setup can efficiently cancel common mode noise from sources such as laser intensity or ambient magnetic-field fluctuations. In single modulation experiments with optical excitation intensity of $\sim$2.02 MW/cm^2, we measured a magnetic field sensitivity of $\sim 4.6 \pm 0.3$ nT/$\sqrt{\text{Hz}}$ using the gradiometer and $\sim 6.7 \pm 0.4$ nT/$\sqrt{\text{Hz}}$ using the single input channel, as shown in Fig. 6.

We performed a double-modulated experiment in which we applied, at the zero crossing of the derivative spectrum, a frequency-modulated microwave excitation with amplitude of 4.5 MHz at various modulation rates from 10 to 100 kHz. An additional oscillating magnetic field of calibrated amplitude at low modulation frequencies from 10 to 200 Hz was applied, in order to simulate an NMR signal.[9] The signal was first demodulated by the lock-in amplifier, and the output of the lock-in amplifier was integrated for 1 sec by the spectrum analyzer. In double modulation experiments, we obtained a magnetic field sensitivity of $\sim 11.9 \pm 0.9$ nT/$\sqrt{\text{Hz}}$ with gradiometer implementation of this technique.

Table I shows the results of performing double-modulation experiments at various frequencies. The sensitivity in double-modulation experiments generally improved as the first modulation rate, i.e., the high frequency modulation rate, increased; this is attributed to the 1/*f* noise of the laser and is the principal advantage of the approach, particularly where low-quality lasers are employed.

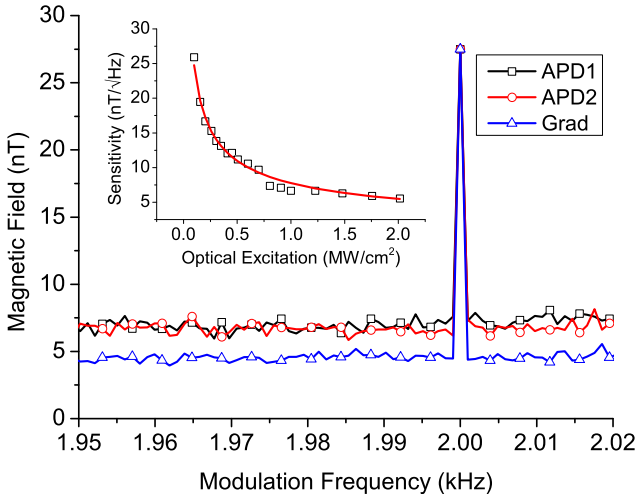

FIG. 6. Magnetic field sensitivity measurements in single modulation mode, using single fluorescence channels, labeled as APD1 and APD2 and a gradiometer with optical excitation intensity of 2.02 MW/cm^2 and microwave Rabi frequency of $\omega_1/2\pi = 1.6$ MHz, with one-second signal integration time. The inset shows the sensitivity as a function of optical excitation intensity using a single channel. Circles indicate measured data, and the solid line is a fit to Eq. (12).

III. TRANSIENT RESPONSE OF THE NV CENTER UNDER CONTINUOUS-WAVE IRRADIATION

A. Bloch-equation model

Since the static magnetic field shifts the transition between $m_s = 0$ and $m_s = +1$ out of resonance with the microwave field, applied to the transition between $m_s = 0$ and $m_s = -1$, the response of an individual NV center to the microwave irradiation can be determined by modeling the center as a set of three two-level systems, with the frequencies of the three systems separated by the hyperfine interaction that couples the electron spin and the ^{14}N nuclear spin. Cross relaxation between the three systems, corresponding to flips of the ^{14}N nucleus, is expected to occur slowly on the time scale of the longitudinal and transverse relaxation of the electron spin toward its steady-state value under laser irradiation. The three two-level systems can thus be considered essentially isolated from each other. We use the Bloch equations, which are valid in the case where the coupling between spins is sufficiently weak that individual spins relax independently,[10] to describe the evolution of each of the two-level systems associated with an NV center, and the response of the NV center is found by summing the responses of the two-level systems.

TABLE I. Magnetic field sensitivity (nT/$\sqrt{\text{Hz}}$) of double modulation technique as a function of low modulation frequency (Hz) at various carrier frequencies (kHz). The optical excitation intensity was 2.3 MW/cm^2, and the microwave-excitation strength corresponded to $\omega_1/2\pi = 1.56$ MHz.

	10.0 Hz	20.0 Hz	50.0 Hz	100.0 Hz	150.0 Hz	200.0 Hz
10.0 kHz	24.0	29.4	22.1	22.2	23.3	29.7
20.0 kHz	20.0	25.4	22.7	20.9	18.5	26.1
50.0 kHz	17.9	20.0	17.6	11.9	16.8	18.4
100.0 kHz	19.1	15.9	15.5	14.3	17.4	17.8

An adaption of the Bloch equations can be used to take account of the fact that thermal relaxation and laser-induced repolarization have opposing effects on longitudinal relaxation. In the reference frame rotating with the resonant component of the microwave field, the evolution equations can be written as

$$\frac{d}{dt}\mathbf{M} = \gamma\mathbf{M}\times\mathbf{B}_{\text{eff}} - \frac{1}{T_{1t}}M_z\mathbf{k} - \frac{1}{T_{1p}}(M_z - M_p)\mathbf{k} - \frac{1}{T_2}(M_x\mathbf{i} - M_y\mathbf{j}), \tag{1}$$

$$= \gamma\mathbf{M}\times\mathbf{B}_{\text{eff}} - \frac{1}{T_1}(M_z - M_0)\mathbf{k} - \frac{1}{T_2}(M_x\mathbf{i} - M_y\mathbf{j}). \tag{2}$$

In Eq. (1), $\mathbf{M}$ is the magnetization, γ is the gyromagnetic ratio of the electron, $\mathbf{B}_{\text{eff}}$ is the effective field in the rotating frame, T_{1t} is the time constant for thermal relaxation toward $M_z = 0$, and T_{1p} is the time constant for repolarization toward $M_z = M_p$, where M_p is the maximum obtainable polarization under optical pumping, and $\mathbf{i}$, $\mathbf{j}$, $\mathbf{k}$ are the unit vectors in the directions x, y, z, respectively. In Eq. (2),

$$T_1 \equiv \left(\frac{1}{T_{1t}} + \frac{1}{T_{1p}}\right)^{-1}$$

and

$$M_0 \equiv \frac{T_{1t}}{T_{1p} + T_{1t}}M_p$$

are effective values of the time constant T_1 for longitudinal relaxation and the steady-state-magnetization M_0. Note that Eq. (2) is a standard way of expressing the Bloch equations.

The resonance frequency ω_0 and the relaxation time constants T_1, T_2 depend on the microscopic environment, which can include modifications of the Hamiltonian induced by strain and temperature, as well as couplings to randomly distributed ^{13}C, paramagnetic nitrogen, and NV centers with other orientations. The values of the parameters ω_0, T_1, T_2 are thus expected to vary across the region probed by the laser. An additional source of inhomogeneity in T_1 and T_2 is variation of beam intensity in this region, due to the Gaussian profile of the beam. While these effects could be modeled and included in an ensemble simulation, our intent here is to present a simple model of the physics that governs the magnetometer's response to a changing field during continuous microwave irradiation, rather than to give a detailed description of the inhomogeneities in the probed region of the diamond.

In order to visualize the way in which magnetometer bandwidth depends on T_1 and T_2, we performed simulations using two-center ensembles. Bloch-equation simulations were compared to experimental curves showing the magnetometer's response as a function of frequency. Two sets of simulations were performed. For the first set, measured values were used for all parameters, aside from a normalization constant that set the amplitude of the low-frequency response to 1. The two centers in a given ensemble had distinct values of

T_1 but identical values for all other parameters. The reason that two values of T_1 were used for these simulations is that biexponential curves were needed to yield good fits to experimental T_1 curves. For these biexponential fits, the initial amplitudes of the two decaying exponentials were equal, to within a few percent, and so the ensemble simulations gave equal weighting to the two NV centers. The resonance frequencies of the simulated two-level systems were chosen to coincide with the measured hyperfine peaks of the ODMR spectrum.

At optical excitation intensity of 0.05 MW/cm^2, the simulated bandwidth measurements matched the experimental data over the full range of microwave powers for which measurements were performed (0.1 MHz $\leq \omega_1/2\pi \leq$ 4 MHz). At higher optical intensities (from 0.30 MW/cm^2 to 1.95 MW/cm^2), the simulated curves matched experimental data only for the lowest microwave powers. Figure 3 compares simulation and experiment for measurements performed with different microwave powers at optical excitation intensity of 1.95 MW/cm^2.

A natural rationalization of these observations is that increasing the laser excitation intensity above 0.05 MW/cm^2 introduces a strong inhomogeneity in the relaxation rates of the NV centers, due to variation in laser intensity across the beam profile, and this inhomogeneity has a significant effect on the magnetometer response when the microwave field is sufficiently strong to excite a substantial fraction of the ensemble. Consistent with this rationalization is the fact that T_1 decreases sharply as the laser excitation intensity is increased from 0.05 MW/cm^2 to 0.30 MW/cm^2. (The best fits of single exponential curves to the experimental T_1 data at these two powers suggest that T_1 decreases by roughly a factor of 5 over this range.)

For a rough characterization of the way in which inhomogeneities in T_1 and T_2 affect the bandwidth, a second set of simulations was performed, using time constants chosen to reproduce the experimental data obtained at the highest laser power and microwave power (shown in Fig. 4). These time constants used in the simulation fall within the range of values that can reasonably be expected for the inhomogeneous distribution at high optical power. These time constants were not selected in a methodical way; rather, they were guesses motivated by inspection of Fig. 3, which shows that the measured values of T_1 and T_2 give a simulated curve that is too flat in the low-frequency region but drops too steeply in the high-frequency region. Increasing the values of T_1 and T_2 for one center and decreasing these values for the other produced a closer fit to the experimental data, as shown in Fig. 4. (The relative population of these two NV centers was chosen so that the simulation matched the experimental data at 1 kHz and 300 kHz.) This simple choice of a two-center ensemble is helpful in visualizing the way in which bandwidth at higher laser power is affected by inhomogeneities in T_1 and T_2.

B. Time constant of the transient response

The Bloch-equation model can be used to find the time constant τ that governs the NV-center response during a continuous-wave (CW) experiment. In the reference frame rotating with the resonant component of the transverse microwave field, the spins evolve under an effective field $\mathbf{B}_{\text{eff}}$ that includes a longitudinal component due to the offset Δ from resonance:

$$-\gamma \mathbf{B}_{\text{eff}} = (\omega_1, 0, \Delta).$$

A weak longitudinal magnetic field oscillating at frequency ω_m in the laboratory frame causes the resonance frequency of the NV center to vary, which in turn causes movement of $\mathbf{B}_{\text{eff}}$. As the effective field moves, the corresponding steady-state solution to the Bloch equations changes as well, both in orientation and magnitude. Throughout the modulation cycle, the magnetization $\mathbf{M}(t)$ relaxes toward the instantaneous steady-state solution $\mathbf{M}_s(t)$. In the limit where the effective field changes slowly, $\mathbf{M}(t) = \mathbf{M}_s(t)$. For higher oscillation frequencies ω_m, where the effective field moves too quickly for $\mathbf{M}(t)$ to relax fully to steady-state, a drop in the magnetometer response is observed.

We show in the appendix that the relaxation of $\mathbf{M}(t)$ in the rotating frame includes a contribution from a transient $\mathbf{M}'_1(t)$ that relaxes without precessing about the effective field, as well as contributions from two linearly independent transients $\mathbf{M}'_2(t)$, $\mathbf{M}'_3(t)$ that precess. If the Rabi frequency $\sqrt{\omega_1^2 + \Delta^2}$ is large compared to ω_m, the precessing transients will not contribute directly to the detected response at frequency ω_m. An additional simplification associated with a large Rabi frequency is that we can approximate $\mathbf{M}'_1(t)$ as evolving independently of the two precessing transients, since interconversion of $\mathbf{M}'_1(t)$ and $\mathbf{M}'_2(t)$, $\mathbf{M}'_3(t)$ is averaged to zero by the fast oscillation of $\mathbf{M}'_2(t)$ and $\mathbf{M}'_3(t)$. A roughly similar mechanism makes adiabatic fast passage[11] possible in NMR: magnetization initially aligned with an effective field will follow the field if it tips slowly, rather than being converted into precessing components perpendicular to the field.

A qualitative understanding of the NV-magnetometer's bandwidth can be obtained from the simplified model in which a single transient $\mathbf{M}'_1(t)$ is continually relaxing in the rotating frame without precessing about the instantaneous effective field. As discussed in the appendix, simulations have validated this model of the magnetometer's response, and physical arguments can be used to obtain an analytic expression for the time constant τ that governs the relaxation of $\mathbf{M}'_1(t)$. When $|\omega_1| \gg T_1^{-1}, T_2^{-1}$, we have

$$\frac{1}{\tau} = \frac{\omega_1^2/T_2 + \Delta^2/T_1}{\omega_1^2 + \Delta^2}, \tag{3}$$

i.e., τ^{-1} is a weighted average of T_1^{-1} and T_2^{-1}, with the weightings determined by the components of the effective field. More generally,

$$\frac{1}{\tau} = \frac{(\omega_1 \cos\varphi)^2/T_2 + \Delta^2/T_1}{(\omega_1 \cos\varphi)^2 + \Delta^2}, \tag{4}$$

where $\omega_1 \cos\varphi$ is the transverse component of $-\gamma \mathbf{B}_{\text{eff}}$ in the vertical plane of the transient. The angle φ can equivalently be defined by the equation

$$\tan\varphi = \frac{\Delta(1/T_2 - 1/T_1)}{(\omega_1 \cos\varphi)^2 + \Delta^2}.$$

When the time scale of the electron-spin relaxation is comparable to the time scale for precession about the resonant transverse component of the microwave field, the term $\cos^2\phi$ in Eq. (4) shifts the weighted average toward T_1^{-1}, increasing the time constant τ. In the experiments performed at low microwave power and high laser power, for example, $\cos^2\varphi \sim 1/4$.

The inverse time constant τ^{-1} gives a rough estimate of the bandwidth, since a distinct drop in the response of a two-level system is expected as the modulation frequency ω_m is increased from a value near zero to $\sim\tau^{-1}$. Numerical tests using the parameters measured at optical excitation intensity of 1.95 MW/cm^2 found that the response of a two-level system drops by $\sim 1/3$ in this range. Although τ^{-1} does not specify the frequency at which the magnetometer response drops by an exact numerical factor, Eqs. (3) and (4) give qualitative insight into the dependence of the magnetometer bandwidth on the time constants for electron-spin relaxation.

IV. SENSITIVITY ANALYSIS

Photon shot noise is an intrinsic noise source that limits the magnetometer's sensitivity. In analyzing magnetic sensitivity in the presence of shot noise, we assume that the ODMR spectrum is a Lorentzian curve and that a small magnetic field $B_z\cos(\omega_m t)$ is measured. The sensitivities of two detection methods are compared. For the single-modulation method, the microwave field is applied at a frequency where the slope of the Lorentzian curve is maximal, and the oscillations of the magnetic field modulate the fluorescence of the NV-center ensemble. For the double-modulation method, frequency modulated microwave field at the modulation rate of ω_c is applied about the peak of the Lorentzian curve, during the detection of the slowly oscillating magnetic field at ω_m, where $\omega_c \gg \omega_m$.

A. Single-modulation method

When the microwave field is tuned to a frequency where the derivative of the Lorentzian spectrum is maximal, the photodiode current corresponding to the detected fluorescence can be expressed as

$$I(t) = I_0 + CB_z\cos(\omega_m t),$$

where

$$C = \frac{dI}{dB} = \frac{3\gamma P_0 R}{4\Delta\omega}\frac{q}{E_p}. \tag{5}$$

In Eq. (5), P_0 is the absorbed power, R is the contrast, $\Delta\omega$ is the spacing between the maximum and minimum points in the derivative of the Lorentzian curve, E_p is the photon energy, and q is the integral of the photodiode current associated with the absorption of a single photon. Shot noise is present in $I(t)$ due to the fact that the photodiode current consists of discrete pulses, where a pulse is associated with the absorption of a photon. The double-sided spectral density of the shot noise associated with the current I_0 is[12]

$$S_n = \frac{P_0}{E_p}q^2. \tag{6}$$

In a phase-sensitive measurement, the noisy signal is multiplied by $\cos(\omega_m t)$ and integrated for a time t_m that corresponds to an integral number of cycles. This measurement procedure can be associated with a linear filter L that gives output

$$f_L(t) = \frac{2}{t_m}\int_{t-t_m}^{t} f(t')\cos[\omega_m(t'-t)]dt'$$

in response to an input function $f(t)$. Formally, we can consider that the measurement is performed by reading the output of this filter at time $t = 0$; note that in the absence of noise, this would produce the value CB_z when $I(t)$ is the input function. We let $n(t)$ represent the shot noise and evaluate the mean-square value of the filtered noise $n_L(t)$ as

$$\langle n_L^2\rangle = \frac{1}{2\pi}\int_{-\infty}^{\infty}|H(\omega)|^2 S_n\, d\omega = S_n\Delta\nu,$$

where $H(\omega)$ is the transfer function of the filter and where the bandwidth is $\Delta\nu = 2/t_m$. Letting the random variable X represent the outcome of the measurement, we define the signal-to-noise ratio (SNR) as

$$\frac{\langle X\rangle}{\sigma_X} = \frac{CB_z}{\sqrt{S_n\ \Delta\nu}}\ . \tag{7}$$

Equation (7) holds for a measurement performed using a single detection channel; for a gradiometer configuration, the shot-noise-limited sensitivity increases by a factor of $\sqrt{2}$. The minimum field $\delta B^{(1)}$ detectable by a gradiometer is found by setting the SNR to 1:

$$\delta B^{(1)} = \frac{4\Delta\omega}{3\gamma R}\sqrt{\frac{1}{Nt_m}}. \tag{8}$$

In Eq. (8), $N = P_0/E_p$ is the number of photons detected per unit time.

B. Double-modulation method

For the double-modulation measurement, the microwave frequency is modulated with amplitude A and frequency $\omega_c \gg \omega_m$ about the peak of the Lorentzian curve. During the measurement, the offset of the microwave field from the peak is

$$\omega(t) = \gamma B_z\cos(\omega_m t + \varphi_m) + A\cos(\omega_c t),$$

where φ_m is a constant that depends on the relative phase of the magnetic field and the carrier wave. When the amplitude A is small enough that the spectrum can be approximated by

a second-degree polynomial over the modulation range, we write the photodiode current as

$$I(t) = I_0 + \frac{8A\gamma P_0 R}{3(\Delta\omega)^2}\frac{q}{E_p}B_z\cos(\omega_m t + \phi_m)\cos(\omega_c t) + \ldots. \quad (9)$$

Demodulation is performed by multiplying $I(t)$ by $\cos(\omega_c t)$ and then using a low-pass filter to remove unwanted frequency components. Phase-sensitive detection at frequency ω_m is then used to measure the amplitude of the demodulated signal

$$I(t) = DB_z\cos(\omega_m t + \phi_m),$$

where

$$D = \frac{2A}{\Delta\omega}\left(\frac{2\gamma P_0 R}{3\Delta\omega}\frac{q}{E_p}\right). \quad (10)$$

In Eq. (10), the terms grouped in parentheses differ by a factor of order unity from C, as defined by Eq. (5), while the ratio outside of the parentheses can be interpreted as the fraction of the linewidth $\Delta\omega$ swept through during the modulation by the carrier wave.

Equation (6) gives the double-sided spectral density of the shot noise $n(t)$ associated with I_0. The noise in the demodulated signal is $n'(t) = n(t)\cos(\omega_c t)$. A simple argument suggests that multiplying $n(t)$ by a sinusoidal function decreases its power spectrum by a factor of 2. Since $n(t)$ is statistically uncorrelated with $\cos(\omega_c t)$,

$$\langle n^2(t)\cos^2(\omega_c t)\rangle = \langle n^2(t)\rangle\langle\cos^2(\omega_c t)\rangle = \frac{1}{2}\langle n^2(t)\rangle.$$

More formally, it can be shown that the power spectrum of $n'(t)$ is

$$S_{n'}(\omega) = \frac{1}{4}[S_n(\omega+\omega_c) + S_n(\omega-\omega_c)] = \frac{1}{2}S_n,$$

where the second equality depends on the fact that S_n is flat in the spectral region of interest. With the outcome of the measurement denoted by random variable Y, arguments similar to those used in obtaining Eq. (7) show that

$$\frac{\langle Y\rangle}{\sigma_Y} = \frac{DB_z}{\sqrt{S_n\Delta\nu/2}}.$$

The minimum detectable field using double modulation with a gradiometer is

$$\delta B^{(2)} = \frac{\Delta\omega}{2A}\left(\frac{3\Delta\omega}{2\sqrt{2}\gamma R}\right)\sqrt{\frac{1}{Nt_m}}. \quad (11)$$

C. Discussion

Equations (8) and (11) can be used to compare the sensitivity of the two measurement methods when photon shot noise is the dominant noise source. For both methods, detection sensitivity depends on the gyromagnetic ratio, the linewidth and contrast of the spectrum, and the rate at which photons are emitted by the ensemble. The SNR of the double-modulation method also depends on the factor $2A/\Delta\omega$. This dependence can be understood by first noting that after a small shift in the magnetic field, the region of the Lorentzian curve swept through during the frequency modulation is shifted as well. The resulting change in the demodulated signal depends strongly on the derivative of the curve at the end points of the frequency sweep, and a large modulation amplitude is needed in order to guarantee that the curve is steep at the end points of the sweep. In particular, an optimal double-modulation measurement must sweep to the peaks of the derivative spectrum, which gives $2A/\Delta\omega = 1$. Note, however, that Eq. (9) is based on the assumption that the derivative varies linearly over the entire range of the frequency sweep. For a sweep with $2A/\Delta\omega = 1$, this model overestimates the magnitude of the derivative at the end points of the sweep by almost a factor of 2. For large modulations, we can thus expect the sensitivity of double modulation to be poorer than would be predicted by Eq. (11). Although the factor $3/2\sqrt{2} \approx 1.1$ in Eq. (11) tends to favor the sensitivity of double modulation, since it is smaller than the corresponding factor 4/3 in Eq. (8), it is reasonable to conclude that the overestimate of the derivative implicit in the derivation of Eq. (11) is more significant than the difference between these numerical factors.

For our experimental tests using a gradiometer configuration, the single-modulation method was more sensitive than the double-modulation method by a factor of 2.5, as described in Sec. II B. Since this difference is larger than would be predicted by Eqs. (8) and (11), even allowing for a correction due to the overestimate of the derivative associated with Eq. (11), it is likely that technical noise was present in the double-modulation experiment, perhaps due to noise at the output of the lock-in amplifier.

In the absence of technical noise, the sensitivity of a magnetometer configured as a gradiometer is frequently limited by the photon shot noise.[5] Under our experimental conditions with optical excitation intensity of $2.02\,\mathrm{MW/cm^2}$, $\Delta\omega/2\pi = 7.5\,\mathrm{MHz}$, $R \sim 0.043$, and detected fluorescence power $\sim 1.0\,\mu\mathrm{W}$, Eq. (8) yields a photon shot-noise limited sensitivity of 4.4 nT for an integration time of $t_m = 1$ sec, approximately the same as our measured sensitivity.

When the sensitivity is limited by the photon shot noise, it should also depend on the optical excitation power as follows:

$$\delta B \propto \sqrt{\frac{1}{N}} \propto \sqrt{1 + \frac{P_{sat}}{P}}, \quad (12)$$

where N is number of photons of the detected signal per unit time, P_{sat} is a characteristic saturation power of the NV defects, and P is the applied optical excitation power.[13] The sensitivity of the NV ensemble to a 2 kHz oscillating magnetic field was measured at various optical excitation intensities from 0.1 to $2.3\,\mathrm{MW/cm^2}$ and showed good agreement (inset in Fig. 6) with Eq. (12).

Further sensitivity improvements will require reducing the shot-noise limit by increasing the signal contrast using

polarization-selective NV excitation,[14] by improving either the detector volume or the collection efficiency,[15] or by using a diamond with more favorable properties, such as longer coherence times or a higher NV^-:NV^0 ratio.

V. CONCLUSION

We have developed an ensemble NV magnetometer for NMR applications, where the magnetometer must detect weak magnetic fields at frequencies ranging from ten to a few hundred kHz. A maximum detection bandwidth of ~1.6 MHz was measured under continuous microwave and optical excitation, limited by the available optical power. A model based on the Bloch equations was used to analyze the response time τ of the NV center, and τ^{-1} was shown to be a weighted average of T_1^{-1} and T_2^{-1}, with the weightings determined by the effective field in the rotating frame. The bandwidth of the magnetometer is thus increased at high optical powers, where optically induced transitions reduce T_1 and T_2. In this regime, the Gaussian profile of the laser beam can introduce significant spatial inhomogeneity in T_1 and T_2.

The optimized sensitivity of our ensemble NV magnetometer is 4.6 ± 0.3 nT/$\sqrt{\text{Hz}}$, which is better by a factor ~5 than the best projected sensitivity for an ensemble NV magnetometer operating at room temperature and close to the sensitivity of a single NV center in isotopically pure diamond. Photon shot noise is the dominant noise source in our measurement. Our results demonstrate that magnetic sensitivity of a few nT at room temperature can be achieved with an ensemble of NV centers in low-cost high-pressure-high-temperature diamond, using a gradiometer configuration that make the measurements robust against most of the experimental noise. The results are promising for the development of affordable, integrated, and portable diamond magnetometers for a variety of magnetic field-sensing applications.

ACKNOWLEDGMENTS

This work was supported by the Director, Office of Science, Office of Basic Energy Sciences, Materials Sciences and Engineering Division, of the U.S. Department of Energy under Contract No. DE-AC02-05CH11231 (all materials, consumables, instrumentation, and salaries except D.B. and V.M.A.). D.B. acknowledges support from the AFOSR/DARPA QuASAR program, IMOD, and the NATO SfP program. We thank J. F. Roch and F. Treussart for the preparation of the diamond sample.

APPENDIX: DERIVATION OF THE TIME CONSTANT FOR THE TRANSIENT RESPONSE

Section III B considers the response of a two-level system to a modulated longitudinal field. When the Rabi frequency is large compared to the modulation frequency ω_m, a simplified model of the evolution can be used to explain the drop in the response as ω_m is increased from zero to $\sim\tau^{-1}$. In this appendix, we present a more formal description of this model and derive Eqs. (3) and (4), which express τ^{-1} as a weighted average of T_1^{-1} and T_2^{-1}.

The Bloch equations can be written in the form

$$\frac{d}{dt}\mathbf{M} = A\mathbf{M} + \mathbf{M}_0, \tag{A1}$$

where

$$A = \begin{bmatrix} -1/T_2 & -\Delta & 0 \\ \Delta & -1/T_2 & -\omega_1 \\ 0 & \omega_1 & -1/T_1 \end{bmatrix}$$

and $\mathbf{M}_0 = [0, 0, M_0]^T$. The general solution to Eq. (A1) is $\mathbf{M} = \mathbf{M}' + \mathbf{M}_s$, where $\mathbf{M}_s$ is the steady-state solution,[11] and where the transient $\mathbf{M}'$ satisfies

$$\frac{d}{dt}\mathbf{M}' = A\mathbf{M}'. \tag{A2}$$

The evolution of $\mathbf{M}'$ can be visualized as involving both precession about the effective field and relaxation toward zero, since Eq. (A2) is equivalent to a set of Bloch equations with $M_0 = 0$. If precession about the effective field is fast compared to relaxation, transients that are initially pependicular to the effective field precess while decaying, but a transient initially aligned with the effective field remains aligned with it during the decay, rather than precessing. More generally, we note that diagonalization of A must yield at least one real eigenvalue λ_1, since the complex eigenvalues of a real matrix come in conjugate pairs. The corresponding unit eigenvector $\mathbf{u}_1$ gives the orientation of a transient that does not precess as it decays. Precessing transients correspond to linear combinations of two eigenvectors $\mathbf{u}_2$, $\mathbf{u}_3$ that have complex eigenvalues and evolve as decaying complex exponentials.

Low-frequency modulation of the magnetic field can be visualized as occurring in a series of short time steps δt_i, each of which begins with a small change in the effective field. Corresponding to the new effective field is a steady-state solution $\mathbf{M}_S$ and a set of eigenvectors $\mathbf{u}_j$. We write

$$\mathbf{M} = \mathbf{M}_s + \sum_{j=1}^{3} a_j \mathbf{u}_j \tag{A3}$$

and note that $a_j\mathbf{u}_j$ represents a decaying transient whose evolution during the time step is determined by the eigenvalue λ_j. In particular, the transients $\mathbf{M}_j'(t)$ referred to in Sec. III B can be identified with the terms $a_j\mathbf{u}_j$ of Eq. (A3).

For each time step, a change in the effective field yields a modified set of eigenvectors, and the three eigenvectors used for time step δt_{i-1} are "mixed" to give the eigenvectors for step δt_i. Each transient is converted by means of this mixing into a linear combination of the three transients present at the end of step δt_{i-1}. In the regime where the precession frequency is large compared to ω_m, however, interconversion of $\mathbf{M}_1'(t)$ and $\mathbf{M}_2'(t)$, $\mathbf{M}_3'(t)$ is averaged to zero by the fast oscillation of $\mathbf{M}_2'(t)$ and $\mathbf{M}_3'(t)$. Since the precessing transients do not contribute to the signal at frequency ω_m, the detected response of the two-level system can be evaluated by replacing Eq. (A3) with

$$\mathbf{M} = \mathbf{M}_s + a_1\mathbf{u}_1. \tag{A4}$$

From Eq. (A4), the response time of the system after a change in the field is

$$\tau = 1/|\lambda_1|.$$

Before deriving a formula for λ_1, we note that simulations have validated the approximate model of the evolution given by Eq. (A4). The evolution is simulated by numerically solving a differential equation that governs the coefficient a_1. In deriving this equation, we assume that the vectors $\mathbf{M}$, $\mathbf{M}_s$, and $\mathbf{u}_1$ are expressed in Cartesian coordinates, and we let $\mathbf{w}$ denote the first row of the change-of-basis matrix that converts Cartesian coordinates into the coordinates a_j defined by Eq. (A3). It follows from Eq. (A4) that

$$a_1 = \mathbf{w}(\mathbf{M} - \mathbf{M}_s). \tag{A5}$$

The differential equation governing a_1 is obtained by summing the changes that occur on the right side of Eq. (A5) during a time step δt. The change in the effective field modifies $\mathbf{M}_s$ and the eigenvectors $\mathbf{u}_j$ without yielding a physical change in the magnetization $\mathbf{M}$. The corresponding contribution to da_1/dt is calculated by differentiating Eq. (A5) while holding $\mathbf{M}$ constant. The physical evolution of $\mathbf{M}$ can be expressed as a simple decay of a_1 toward zero with rate constant $|\lambda_1|$. The differential equation obtained by summing these changes is

$$\frac{d}{dt}a_1 = a_1\left(\frac{d}{dt}\mathbf{w}\right)\mathbf{u}_1 + \mathbf{w}\left(a_1\mathbf{u}_1 + \mathbf{M}_s - \frac{d}{dt}\mathbf{M}_s\right) + \lambda_1 a_1. \tag{A6}$$

In numerical tests using parameters similar to those measured for the experiments performed at laser power 1.95 MW/cm^2, simulations based on Eq. (A6) matched Bloch-equation simulations up to frequences of a few hundred kHz, with the exact range of validity depending on the magnitude of the microwave field and the offset from resonance.

To derive a formula for λ_1, we analyze the exponential decay of the transient $a_1\mathbf{u}_1$ in a reference frame where the transient lies in the xz plane. Within this frame, the effective field is expressed as

$$-\gamma\mathbf{B}_{\text{eff}} = (\omega_1\cos\varphi, \omega_1\sin\varphi, \Delta).$$

The evolution during δt can be visualized as occuring in three steps:

1. The x component and z component of the transient are multiplied by $(1 - \delta t/T_2)$ and $(1 - \delta t/T_1)$, respectively.
2. The transient precesses about the y-component of $\mathbf{B}_{\text{eff}}$.
3. The transient precesses about the component of $\mathbf{B}_{\text{eff}}$ lying in the xz plane.

Since the transient decays without precessing, the summed changes associated with these three steps must leave its orientation unchanged. Note that the transient remains in the xz plane during the first two steps; precession about a field component in the xz plane during step three will thus rotate it out of the xz plane and away from its initial orientation, unless the transient is aligned with the field component in this plane. It follows that

$$a_1\mathbf{u}_1 \propto (\omega_1\cos\varphi, 0, \Delta).$$

Given this orientation for the transient, we find that the combined effects of longitudinal and transverse relaxation during δt change its magnitude by a factor $(1 - \delta t/\tau)$, where

$$\frac{1}{\tau} = \frac{(\omega_1\cos\varphi)^2/T_2 + \Delta^2/T_1}{(\omega_1\cos\varphi)^2 + \Delta^2}. \tag{A7}$$

Equation (A7) expresses τ^{-1} as a weighted average of T_1^{-1} and T_2^{-1}, with the weightings determined by the components of the effective field in the vertical plane of the transient.

The angle φ appearing in Eq. (A7) is determined by the requirement that precession about the y-component of $\mathbf{B}_{\text{eff}}$ compensate for any change in the orientation of the transient due to the different relaxation rates of its longitudinal and transverse components. When $\omega_1 \gg T_1^{-1}, T_2^{-1}$, we have $\varphi \approx 0$, and Eq. (A7) reduces to

$$\frac{1}{\tau} = \frac{\omega_1^2/T_2 + \Delta^2/T_1}{\omega_1^2 + \Delta^2}.$$

More generally, the longitudinal and transverse relaxation changes the orientation of the transient by an angle

$$\alpha = \frac{(\Delta\omega_1\cos\varphi)(1/T_2 - 1/T_1)}{(\omega_1\cos\varphi)^2 + \Delta^2}\ \delta t.$$

Setting $\alpha = (\omega_1\sin\varphi)\delta t$ shows that φ satisfies the equation

$$\tan\varphi = \frac{\Delta(1/T_2 - 1/T_1)}{(\omega_1\cos\varphi)^2 + \Delta^2}. \tag{A8}$$

The dependence of φ on ω_1, Δ, T_1, and T_2 can be visualized by solving Eq. (A8) graphically. The right side of the equation defines a curve that oscillates between minima at $\varphi = N\pi$ and maxima at $\varphi = N\pi/2$, and the parameters of the two-level system affect φ by determining the detailed form of this curve.

[1]Y.-R. Chang, H.-Y. Lee, K. Chen, C.-C. Chang, D.-S. Tsai, C.-C. Fu, T.-S. Lim, Y.-K. Tzeng, C.-Y. Fang, C.-C. Han, H.-C. Chang, and W. Fann, Nat. Nanotechnol. **3**, 284 (2008).
[2]M. Börsch and J. Wrachtrup, Chem. Phys. Chem. **12**, 542 (2011).
[3]G. Balasubramanian, P. Neumann, D. Twitchen, M. Markham, R. Kolesov, N. Mizuochi, J. Isoya, J. Achard, J. Beck, J. Tissler, V. Jacques, P. R. Hemmer, F. Jelezko, and J. Wrachtrup, Nature Mater. **8**, 383 (2009).
[4]S. Steinert, F. Dolde, P. Neumann, A. Aird, B. Naydenov, G. Balasubramanian, F. Jelezko, and J. Wrachtrup, Rev. Sci. Instrum. **81**, 043705 (2010).
[5]V. M. Acosta, E. Bauch, A. Jarmola, L. J. Zipp, M. P. Ledbetter, and D. Budker, Appl. Phys. Lett. **97**, 174104 (2010).
[6]R. S. Schoenfeld and W. Harneit, Phys. Rev. Lett. **106**, 030802 (2011).
[7]P. Neumann, J. Beck, M. Steiner, F. Rempp, H. Fedder, P. R. Hemmer, J. Wrachtrup, and F. Jelezko, Science **329**, 542 (2010).

[8]V. M. Acosta, E. Bauch, M. P. Ledbetter, C. Santori, K.-M. C. Fu, P. E. Barclay, R. G. Beausoleil, H. Linget, J. F. Roch, F. Treussart, S. Chemerisov, W. Gawlik, and D. Budker, Phys. Rev. B **80**, 115202 (2009).
[9]M. P. Ledbetter, C. W. Crawford, A. Pines, D. E. Wemmer, S. Knappe, J. Kitching, and D. Budker, J. Magn. Reson. **199**, 25 (2009).
[10]R. K. Wangsness and F. Bloch, Phys. Rev. **89**, 728 (1953).
[11]M. Goldman, *Quantum Description of High-Resolution NMR in Liquids* (Clarendon, 1991), Chap. 1.
[12]W. B. Davenport Jr. and W. L. Root, *An Introduction to the Theory of Random Signals and Noise*, 1st ed. (Wiley-IEEE, 1987), Chap. 7.
[13]C. Kurtsiefer, S. Mayer, P. Zarda, and H. Weinfurter, Phys. Rev. Lett. **85**, 290 (2000).
[14]T. P. M. Alegre, C. Santori, G. Medeiros-Ribeiro, and R. G. Beausoleil, Phys. Rev. B **76**, 165205 (2007).
[15]L. M. Pham, D. Le Sage, P. L. Stanwix, T. K. Yeung, D. Glenn, A. Trifonov, P. Cappellaro, P. R. Hemmer, M. D. Lukin, H. Park, A. Yacoby, and R. L. Walsworth, New J. Phys. **13**, 045021 (2011).